Stem Cell Reports
Report
OPEN ACCESS

Vitamin C and L-Proline Antagonistic Effects Capture Alternative States in the Pluripotency Continuum

Cristina D'Aniello,[1] Ehsan Habibi,[2] Federica Cermola,[1] Debora Paris,[3] Francesco Russo,[4] Alessandro Fiorenzano,[1] Gabriele Di Napoli,[1] Dominique J. Melck,[3] Gilda Cobellis,[5] Claudia Angelini,[4] Annalisa Fico,[1] Robert Blelloch,[6] Andrea Motta,[3] Hendrik G. Stunnenberg,[2] Dario De Cesare,[1,*] Eduardo J. Patriarca,[1] and Gabriella Minchiotti[1,*]

[1]Stem Cell Fate Laboratory, Institute of Genetics and Biophysics, 'A. Buzzati-Traverso', CNR, 80131 Naples, Italy
[2]Department of Molecular Biology, Radboud University, Faculty of Science, Radboud Institute for Molecular Life Sciences, 6525 GA Nijmegen, the Netherlands
[3]Institute of Biomolecular Chemistry, CNR, 80078 Pozzuoli (Napoli), Italy
[4]Institute for Applied Mathematics "Mauro Picone", CNR, 80131 Naples, Italy
[5]Department of Biophysics, Biochemistry and General Pathology, Second University of Naples, 80138 Naples, Italy
[6]Department of Urology, The Eli and Edythe Broad Center of Regeneration Medicine and Stem Cell Research, Center for Reproductive Sciences, University of California, San Francisco, San Francisco, CA 94143, USA
*Correspondence: dario.decesare@igb.cnr.it (D.D.C.), gabriella.minchiotti@igb.cnr.it (G.M.)
http://dx.doi.org/10.1016/j.stemcr.2016.11.011

SUMMARY

Metabolites and cofactors are emerging as key regulators of cell plasticity and reprogramming, and their role in the control of pluripotency is just being discovered. Here we provide unprecedented evidence that embryonic stem cell (ESC) pluripotency relies on the relative levels of two physiological metabolites, namely ascorbic acid (vitamin C, VitC) and L-proline (L-Pro), which affect global DNA methylation, transcriptional profile, and energy metabolism. Specifically, while a high VitC/L-Pro ratio drives ESCs toward a naive state, the opposite condition (L-Pro excess) captures a fully reversible early primed pluripotent state, which depends on autocrine fibroblast growth factor and transforming growth factor β signaling pathways. Our findings highlight the pivotal role of metabolites availability in controlling the pluripotency continuum from naive to primed states.

INTRODUCTION

Pluripotency is transiently induced during the early stages of mammalian embryo development. Blastocyst stem cells progress from a "naive/ground" state to a "primed" state of pluripotency before lineage commitment (Martinez Arias et al., 2013). Two distinct pluripotent stem cells, embryonic stem cells (ESCs) and epiblast stem cells (EpiSCs), are considered as their in vitro counterparts. ESCs and EpiSCs differ with respect to their morphology, metabolism, DNA methylation levels, transcription profiles, and growth factors requirement (Weinberger et al., 2016). Pluripotency states are unstable and thus difficult to stabilize in vitro. Indeed, ESC cultures consist of heterogeneous cells dynamically fluctuating between different pluripotent states (Hayashi et al., 2008; Toyooka et al., 2008). EpiSCs frequently lose the primed state, acquiring features of late pre-gastrula embryos (Wu and Izpisua Belmonte, 2015). Known molecular determinants of such plasticity are mainly transcription factors, while the role of metabolism has been largely unexplored until recently. Indeed, it has now become evident that metabolites, including amino acids, act as key regulators of pluripotent stem cell plasticity and behavior. For instance, it has been shown that ESC self-renewal depends on L-threonine (Wang et al., 2009), while ESC identity is regulated by L-proline (L-Pro) availability (Casalino et al., 2011; Comes et al., 2013; D'Aniello et al., 2015; Washington et al., 2010). Moreover, several metabolites act as epigenetic signals (Blaschke et al., 2013; Comes et al., 2013; Shyh-Chang et al., 2012), thus defining a regulatory network among metabolism, epigenetic modification, and pluripotency, knowledge of which is still limited (Harvey et al., 2016). Here we provide evidence that pluripotency is finely controlled by the mutual availability of two physiological metabolites, vitamin C (VitC) and L-Pro, and propose that naive and early primed pluripotency states can be captured in vitro by exploiting the epigenetic activity of these metabolites.

RESULTS

Vitamin C and L-Proline Induce Opposite Effects on DNA Methylation in ESCs

Recent evidence from our laboratory demonstrates that ESCs suffer a highly specific intrinsic shortage of the nonessential amino acid L-Pro, which induces the amino acid stress response pathway (D'Aniello et al., 2015). Exogenously provided L-Pro alleviates this stress condition and converts round-shaped ESCs into flat-shaped pluripotent stem cells. This phenotypic transition is fully reversible, either after L-Pro withdrawal or by addition of VitC (Casalino et al., 2011; Comes et al., 2013), raising the hypothesis that these two metabolites play antagonistic roles in

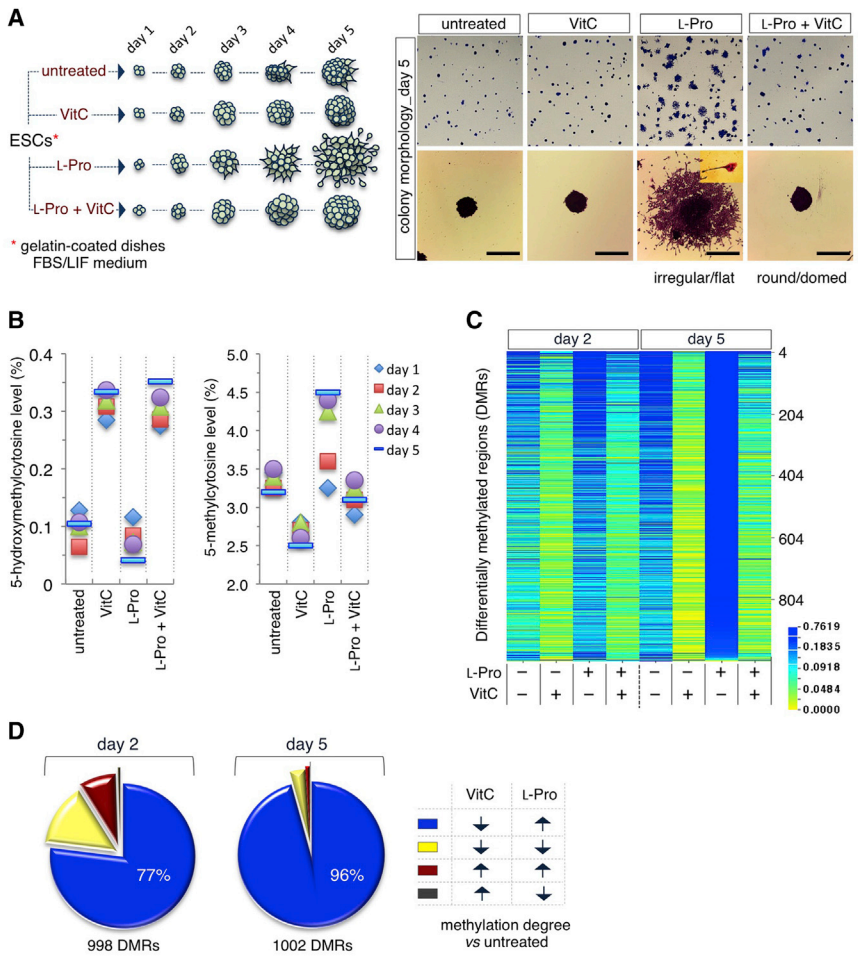

Figure 1. Vitamin C and L-Proline Induce Opposite Effects on DNA Methylation in ESCs

(A) Schematic representation of the time-course colony assay. FBS/LIF ESCs plated at low density ± VitC (500 μM)/± L-Pro (150 μM) for 5 days (left panel). Representative pictures of crystal violet-stained colonies (right panels). Scale bars, 250 μm.

(B) Time-course mass spectrometry (MS) analysis of 5hmc and 5mc levels in ESCs ± VitC (500 μM)/± L-Pro (150 μM). Data are relative levels (%) compared with day 1.

(C) Heatmap (CIMminer, http://discover.nci.nih.gov/cimminer/) showing the differentially methylated regions (DMRs) in ESCs ± VitC (500 μM)/± L-Pro (150 μM) at days 2 and 5.

(D) Pie graphs showing the percentage of DMRs shared by VitC- and L-Pro-treated ESCs at days 2 and 5.

See also Figure S1.

controlling ESC identity. VitC is the most relevant naturally occurring reducing agent and enhances the catalytic activity of 2-oxoglutarate/Fe(II)-dependent dioxygenases, including TET DNA demethylases, and thereby contributes to epigenetic regulation, cell differentiation, and reprogramming (Hore et al., 2016; Krishnakumar and Blelloch, 2013; Monfort and Wutz, 2013). We thus reasoned that VitC and L-Pro might regulate pluripotency by exerting opposite effects on the dynamics of DNA methylation. We first quantified DNA methylation levels in ESCs treated with L-Pro ± VitC at different time points by liquid chromatography followed by mass spectrometry (LC-MS) (Figures 1A and 1B). VitC supplementation led to a rapid and sustained increase of 5-hydroxymethylcytosine (5hmC) and reduced 5-methylcytosine (5mC) levels. Conversely, supplemental L-Pro increased 5mC and reduced 5hmC levels, and its effect was fully counteracted by VitC (Figure 1B). We then compared genome-wide methylation profiling of ESCs ± L-Pro and ESCs, ± VitC, at days 2 and 5 of treatment. Reduced representation bisulfite sequencing (RRBS) analysis identified ~1,000 differentially methylated regions (DMRs) distributed throughout all chromosomes (Figure 1C and Table S1). The methylation levels of individual CpGs were highly correlated ($r > 0.9$) between the different groups (Figures S1A and S1B). Interestingly, the majority of DMRs (77% at day 2 and 96% at day 5) that were hypomethylated in VitC-treated ESCs were conversely hypermethylated in L-Pro-treated ESCs (Figures 1D and S1C), thus indicating that VitC and L-Pro modulate methylation at the same DNA regions in an opposite manner. Of note, a high fraction of DMRs (50%) lay in promoters (mostly HCPs) and ~20% in enhancers (Figures S1D and S1E; Table S1). Moreover, DMR-associated genes are highly enriched in genes related to the developmental process ($p = 6.3 \times 10^{-38}$) and DNA-binding transcriptional regulators ($p = 9.7 \times 10^{-34}$) (Table S1). Our findings provide evidence that L-Pro availability regulates DNA methylation in ESCs. Of note, DNA methylation levels increase in the transition from naive to primed pluripotency (Maruotti et al., 2010), thus leading to the hypothesis that the antagonistic effects of VitC and L-Pro on the DNA methylation pattern might regulate pluripotency.

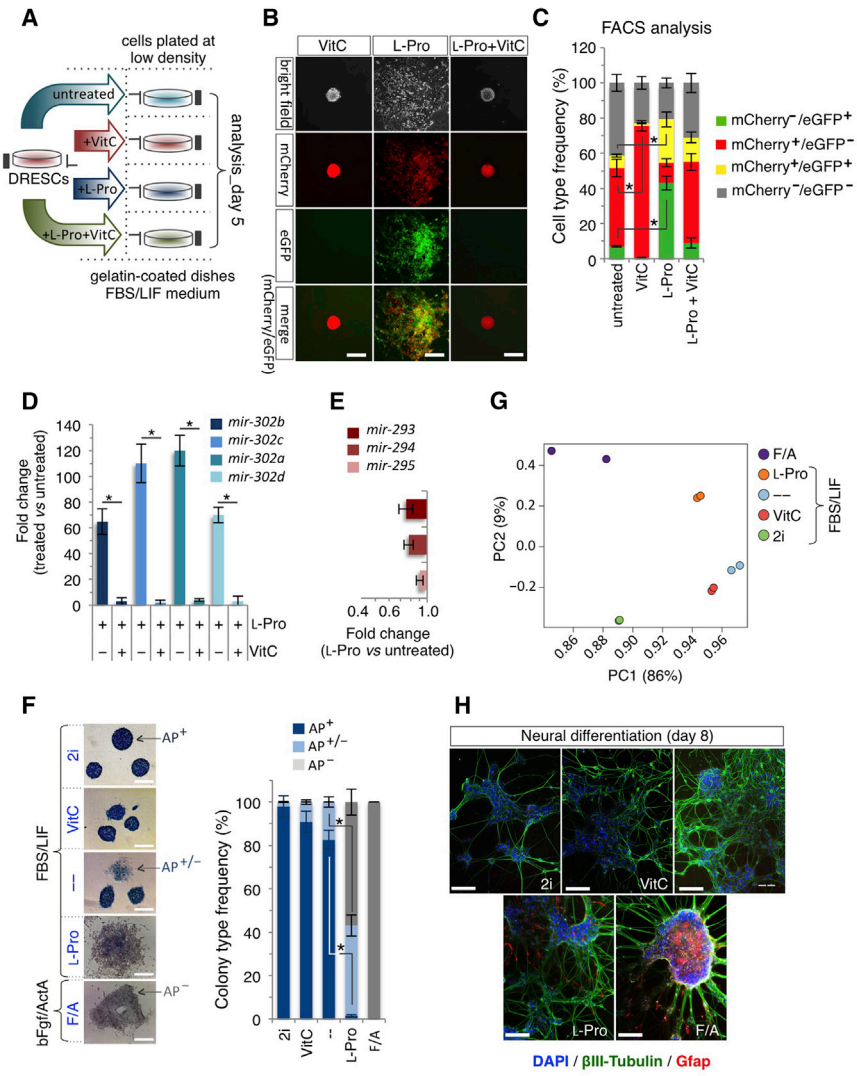

Figure 2. Molecular and Pluripotency Features of Vitamin C- and L-Proline-Induced Cells

(A) Schematic representation of the experimental strategy. Dual-reporter ESCs (DRESCs) plated at low density ± VitC (500 μM)/± L-Pro (150 μM) and analyzed at day 5.

(B) Representative bright-field and fluorescence images of colonies generated from DRESCs ± VitC (500 μM)/± L-Pro (150 μM) at day 5. Red (*mir-290*), green (*mir-302*), and yellow (*mir-290* and *mir-302*) signals indicate expression of the transgenes. Scale bars, 250 μm.

(C) Fluorescence-activated cell sorting (FACS) quantification of mCherry$^{\pm}$/eGFP$^{\pm}$ cells in DRESCs ± VitC (500 μM)/± L-Pro (150 μM). Data are mean ± SEM; *p < 0.01 (n = 3 independent experiments).

(D) qPCR analysis of *mir-302* expression in L-Pro (150 μM) ± VitC (500 μM)-treated ESCs at day 5. Data are fold change in gene expression compared with control, normalized to *Gapdh*, and are mean ± SEM; *p < 0.005 (n = 3 independent experiments).

(E) qPCR analysis of *mir-290* expression in L-Pro-treated ESCs (150 μM) at day 5. Data are fold change versus control, normalized to *Gapdh*, and are mean ± SEM (n = 3 independent experiments).

(F) Representative pictures (left) and frequency (right) of AP^{+}, AP$^{+/-}$, and AP^{-} staining on colonies derived from ESCs plated at low density in the presence of the indicated inhibitors, metabolites, and growth factors. Data are mean ± SEM; *p < 0.05 (n = 3 independent experiments). Scale bars, 250 μm.

(G) Principal component (PC) analysis of RNA-sequencing data generated from ESCs grown as indicated in (F).

(H) Representative pictures of βIII-tubulin (green) and GFAP (red) immunofluorescence on neurons derived from ESCs grown as in (F). Nuclei are stained with DAPI. Scale bars, 100 μm.

See also Figure S2.

Vitamin C and L-Proline Modify *mir-290/mir-302* Signature in ESCs

Pluripotent stem cell transition from naive to primed state is marked by changes in the expression of the *mir-290* and *mir-302* clusters, which correspond to naive (pre-implantation epiblast) and primed (late post-implantation epiblast of the pre-gastrulating embryo) states, respectively; whereas co-expression of the two clusters identifies an intermediate (early post-implantation epiblast) state (Parchem et al., 2014). To assess whether VitC and L-Pro impact on the expression of these microRNA clusters, we exploited the potential of ESCs carrying the reporters for the *mir-290* and *mir-302* loci (*mir-290*_mCherry/*mir-302*_eGFP dual-reporter ESCs, named DRESCs) (Parchem et al., 2014). Addition of VitC to fetal bovine serum (FBS)/leukemia inhibitory factor (LIF) DRESCs increased the fraction of mCherry^{+}/eGFP^{-} (red) cells at the expense of mCherry$^{\pm}$/eGFP^{+} cells (yellow and green) (Figures 2A–2C). A similar effect was observed in feeder-dependent FBS/LIF culture conditions (Figures S2A–S2C). Conversely, L-Pro supplementation increased the frequency of mCherry^{+}/eGFP^{+} (yellow) and mCherry^{-}/eGFP^{+} (green) cells (Figures 2A–2C), and its effect was fully reversed by VitC (Figures 2A–2C). Accordingly, the expression of all members of the *mir-302-367* cluster, and the *pri-mir-302* was strongly induced in L-Pro-treated ESCs (Figures 2D,

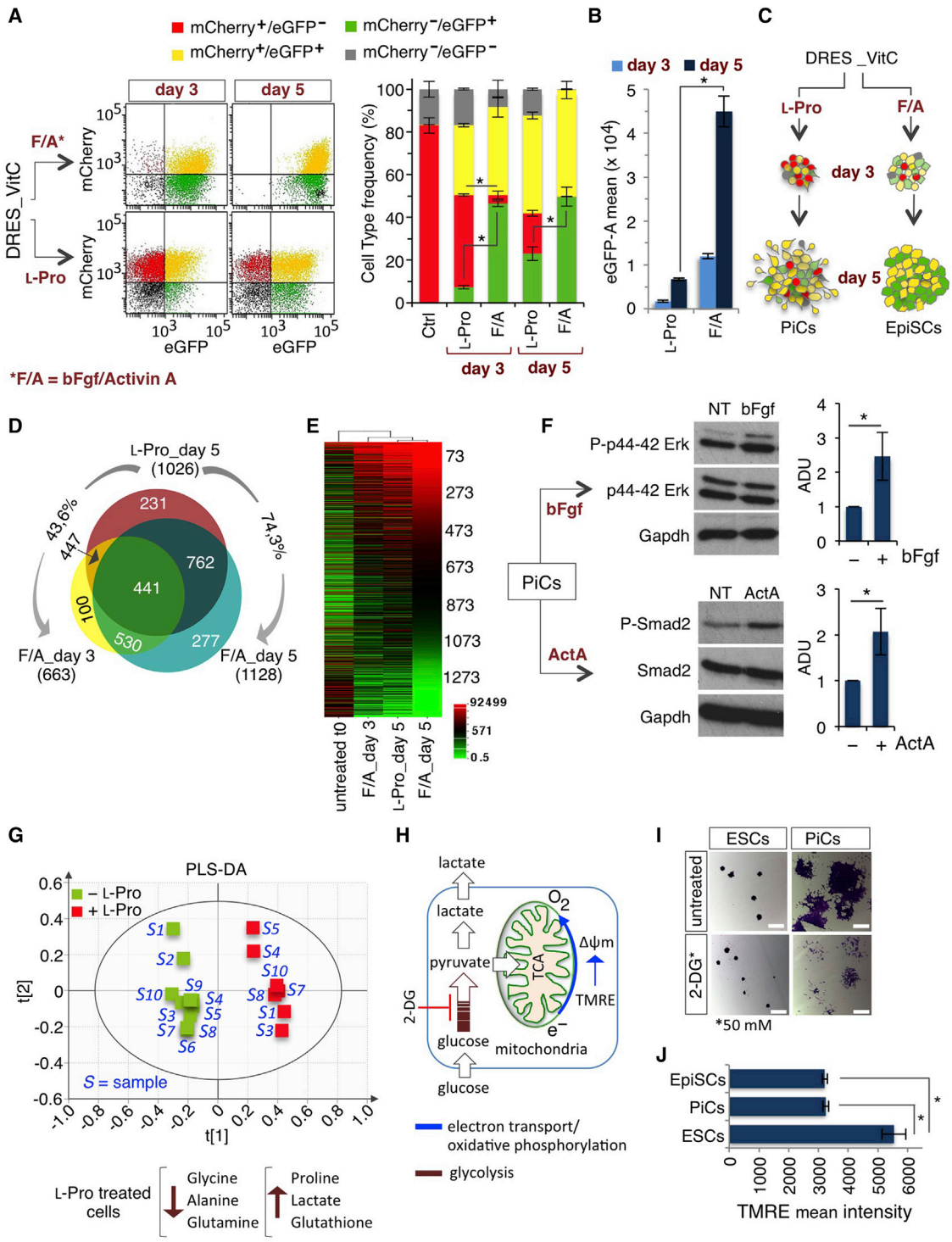

Figure 3. L-Proline Mimics bFGF/Activin A Treatment in ESCs

(A and B) DRESCs were passaged three times in VitC (100 μM), plated at low density and treated with either L-Pro (1 mM) or F/A and analyzed at days 3 and 5. Representative FACS plots (A, left panels) and quantification (A, right panel) of mCherry$^{\pm}$/eGFP$^{\pm}$ cell distribution. Quantification of eGFP intensity mean (B). Data are mean ± SEM; *p < 0.001 (n = 3 independent experiments).

(C) Schematic representation of eGFP/mCherry-positive cells' distribution in colonies from L-Pro- and F/A-treated DRESCs.

(legend continued on next page)

S2D, and S2E), whereas VitC blocked L-Pro-dependent induction of *mir-302* (Figure 2D). Of note, expression of *mir-290* cluster persisted, though to a reduced extent in L-Pro-treated cells (Figure 2E). Our findings suggest that FBS/LIF ESCs supplemented with either VitC or L-Pro acquire a naive (*mir-290*$^{+}$/*mir-302*$^{-}$) and a primed (*mir-290*$^{\pm}$/*mir-302*$^{+}$) signature, respectively.

Molecular and Pluripotency Features of Vitamin C- and L-Proline-Induced Cells

To further support our findings, we compared VitC- and L-Pro-treated ESCs with naive/LIF/2i and primed/basic fibroblast growth factor (bFGF)/Activin A (F/A) cells, respectively. Interestingly, the percentage of round/domed-shaped and alkaline phosphatase-positive (AP^{+}) colonies increased in 2i and VitC culture conditions compared with control, which, as expected, showed some irregular colonies with an intermediate AP staining (AP$^{+/-}$) (Figure 2F). Conversely, flat-shaped F/A EpiSC colonies were AP negative. Interestingly, the large majority ($\geq$90%) of L-Pro-induced flat-shaped colonies were either AP$^{+/-}$ or AP^{-} (Figure 2F). To further investigate this phenotype, we compared the transcriptome profiling of FBS/LIF ± VitC or L-Pro, naive/2i, and F/A EpiSCs, and identified ~7,900 deregulated genes in the different conditions (fold change [FC] $\geq$ 2; $p < 0.05$). Interestingly, principal component analysis placed VitC between 2i and untreated control, and L-Pro between control and F/A (Figure 2G). Accordingly, a set of pluripotency-associated genes was upregulated in 2i and VitC conditions but downregulated in L-Pro and F/A compared with control. Conversely, priming markers showed the opposite trend (Figure S2F and Table S2). Consistent with these findings, the four cell populations significantly differ in their differentiation potential. Indeed, only L-Pro- and F/A-derived neural cell populations already showed complex βIII-tubulin^{+} structures at an early time, and stained positive for the late glial marker glial fibrillary acidic protein (GFAP) (Figure 2H) (Fico et al., 2008). These data suggest that VitC and L-Pro captured alternative pluripotency states placed between the naive/2i (Habibi et al., 2013) and primed/F/A.

L-Proline and F/A Capture Distinct Temporal Stages of Primed Pluripotency

To further compare the effect of L-Pro and F/A, we analyzed the distribution of mCherry$^{\pm}$/eGFP$^{\pm}$ cells in VitC/DRESCs upon treatment with either L-Pro or F/A. Interestingly, mCherry^{+}/eGFP^{+} (yellow) and mCherry^{-}/eGFP^{+} (green) cells strongly and progressively increased in both L-Pro- and F/A-treated ESCs at the expense of the mCherry^{+}/eGFP^{-} (red) population (Figure 3A). However, the extent of L-Pro and F/A activity was different. Specifically, the percentage of mCherry^{-}/eGFP^{+} (green) cells almost doubled in F/A-treated compared with L-Pro-treated cells and mCherry^{+}/eGFP^{-} (red) cells persisted, although at a low level, only in L-Pro-treated DRESCs (day 5, Figure 3A). Furthermore, eGFP fluorescence intensity was higher (~4-fold) in F/A compared with L-Pro (Figure 3B). In line with these findings, markers of the late epiblast (*Brachyury*, *Cerberus*, and *Sox17*) were induced by L-Pro, although at lower levels compared with F/A (Figure S3A). Finally, although the fraction of mCherry^{+}/eGFP^{+} (*yellow*) cells was comparable, the *mir-302/mir-290* expression ratio was ~10-fold higher in F/A compared with L-Pro (Figure S3B). To further explore the possibility that L-Pro and F/A induced distinct temporal stages of primed pluripotency, we compared the transcriptome profiling of the L-Pro and F/A mCherry^{+}/eGFP^{+} (yellow) population, and found >1,000 genes deregulated compared with mCherry^{+}/eGFP^{-} (red) control cells (NoiSeq; posterior probability > 0.99; FC $\geq$ 4; Table S3). The two populations shared up to 75% of common genes (Figure 3D) with the same deregulation trend (Figure 3E) but

(D) Venn diagram showing the overlap between differentially expressed genes in mCherry^{+}/eGFP^{+} (yellow) cells from L-Pro-treated (day 5) and F/A-treated (days 3 and 5) DRESCs. Relative expression of each gene was normalized to untreated cells.

(E) Heatmap representation of genes deregulated in L-Pro-treated (day 5) and F/A-treated (days 3 and 5) cells compared with control.

(F) Western blot analysis of phospho-Erk/Erk (upper panels) and phospho-Smad2/Smad2 (lower panels) in L-Pro-induced cells (PiCs) treated with ±bFGF (12 ng/mL) and ±Activin A (20 ng/mL) (15 min), respectively. Anti-Gapdh antibody was used as loading control. Densitometric analysis (arbitrary densitometry units [ADU]) is shown as pErk/Erk and pSmad2/Smad2 ratio. Data are mean ± SEM; *$p < 0.01$ (n = 3 independent experiments).

(G) Projection to latent structure-discriminant analysis (PLS-DA) score plot showing the projection of all the spectral classes analyzed (−L-Pro, green boxes; and +L-Pro, red boxes). The model quality is evaluated by the goodness of fit and the goodness of prediction, represented by parameters R2Y = 0.98 and Q2 = 0.96. Classes are separated along the first principal component t[1], which represents interclass variation. The second component t[2] accounts for intraclass variation.

(H) Schematic representation of the oxidative phosphorylation (blue) and glycolysis (red) metabolic pathways.

(I) Representative phase-contrast images of ESC and PiC colonies (day 5), and ±2-DG (50 mM; 16 hr), stained with crystal violet. Scale bars, 200 μm.

(J) Tetramethylrhodamine (TMRE) mean intensity in ESCs, EpiSCs, and PiCs at day 5. Data are mean ± SEM; *$p < 0.05$ (n = 3 independent experiments).

See also Figure S3.

different magnitudes. Specifically, pluripotency-associated genes were downregulated either at similar level (*Nanog*, *Klf2*, *Klf4*, and *Gbx2*) or at lower levels (up to 10-fold) (*Dppa 2*, *3*, *4*, *5a*, *Rex1*, *Esrrb*) in F/A- compared with L-Pro-treated cells (Figure S3C and Table S3). Furthermore, mesendodermal-related genes (e.g., *Brachyury*, *Cer1*, *Dkk1*, *Eomes*, *Foxa2*, and *Sox17*) were induced at higher levels in F/A than in L-Pro (Figure S3D and Table S3). We then asked whether L-Pro-induced cells (PiCs) were still responsive to F/A. Both Erk and Smad2 phosphorylation was induced in PiCs upon addition of either bFGF or activin (Figure 3F), and mCherry$^+$/eGFP$^+$ (yellow) and mCherry$^-$/eGFP$^+$ (green) cells increased at the expense of mCherry$^+$/eGFP$^-$ (red) cells (Figure S3E). In addition, mean eGFP intensity also increased in F/A-treated PiCs (Figure S3E). These data indicate that L-Pro and F/A similarly induce a naive to primed transition and further suggest that L-Pro captures an earlier primed state.

L-Proline Induces a Metabolic Reprogramming in ESCs

One of the earliest events that occur in the transition from naive to primed pluripotency is a switch from a bivalent to exclusively glycolytic metabolism (Zhou et al., 2012). We thus performed a nuclear magnetic resonance (NMR)-based global metabolomic profiling of ESCs ± L-Pro and found strong differences in their metabolite content (Figure 3G and Table S4). In particular, PiCs showed increased levels of L-Pro and reduced levels of different amino acids (L-Gln, L-Tyr, L-Gly, L-Ala L-Val, L-Leu, L-Ser) (Table S4), in line with our previous findings that L-Pro supplementation inactivates the amino acid stress response pathway in ESCs (D'Aniello et al., 2015). Remarkably, lactate levels significantly increased (Figures 3G, 3H, and S3F; Table S4) and PiCs were more susceptible to the glycolysis inhibitor 2-deoxy-D-glucose (2-DG) compared with ESCs (Figures 3H, 3I, and S3G), suggesting a metabolic shift to glycolysis. Moreover, the mitochondrial membrane potential was significantly reduced in PiCs as in F/A EpiSCs compared with ESCs (Figure 3J), indicating that oxidative phosphorylation was reduced, and further supporting the idea that PiCs undergo a metabolic reprogramming, which resembles the one occurring in the naive to primed transition (Zhou et al., 2012).

L-Proline-Induced Primed State Depends on Autocrine FGF and TGF-β Signaling Pathways

To further explore the notion that L-Pro and F/A exert similar effects on ESCs, we first evaluated whether L-Pro induced Erk (FGF) and Smad2 (transforming growth factor β [TGF-β]) signaling pathways in FBS/LIF ESCs. Interestingly, both Erk and Smad2 phosphorylation were induced by supplemental L-Pro (Figure 4A). Furthermore, L-Pro-induced phenotypic transition was impaired in the presence of FGF and TGF-β chemical inhibitors PD0325901 and SB431542, respectively. Indeed, while L-Pro-treated cells generated only 15% of domed colonies, domed-shaped mCherry$^+$/eGFP$^-$ (red) colonies increased up to 70% in the presence of PD0325901 or SB431542, even with high doses of L-Pro (Figures 4B and 4C). Moreover, gene ontology analysis revealed that the transcriptome of both L-Pro- and F/A-derived mCherry$^+$/eGFP$^+$ (yellow) cells was highly enriched in genes of Erk superpathway (Figures 4D and 4E; Table S3). These data suggested that L-Pro drives naive ESCs toward a primed state of pluripotency by inducing and sustaining autocrine FGF and TGF-β signaling.

DISCUSSION

The naive to lineage primed transition was proposed as a gradual continuum of pluripotent states with distinct functional and transcriptional signatures and biases (Tesar, 2016). Several stem cell types with different degrees of pluripotency can be established under artificial culture conditions (Wu and Izpisua Belmonte, 2015). Specifically, naive and primed (EpiSCs) cells rely on chemical inhibitors (2i) or growth factors (F/A), respectively, and are largely used as in vitro models of pluripotency. Here we provide evidence that the relative levels of two physiological metabolites, namely VitC and L-Pro, push FBS/LIF ESCs toward naive (low L-Pro/high VitC) or early primed (high L-Pro/low VitC) states, between naive/2i and F/A primed states of the pluripotency continuum. In particular, similarly to the F/A primed state (EpiSCs), the high L-Pro/low VitC condition is associated with a metabolic reprogramming toward glycolysis and is strictly dependent on the activation and maintenance of autocrine bFGF and TGF-β signaling pathways. Interestingly, while F/A EpiSCs show molecular features of late pre-gastrulation epiblast and are difficult to revert to naive ESCs (Guo et al., 2009), PiCs display molecular, metabolic, and functional features (Table S5) of a transitional/reversible primed state in the pluripotency continuum, which has been hypothesized to define the boundary beyond which the transition becomes irreversible (Hackett and Surani, 2014; Martello and Smith, 2014). Of note, our findings indicate that VitC and L-Pro are both limiting in ESCs even in complete FBS/LIF culture conditions. This is in line with our recent findings that an autoregulatory loop limits L-Pro biosynthesis in ESCs (D'Aniello et al., 2015); nevertheless, whether and how intracellular levels of VitC are regulated in ESCs is still unknown and deserves further investigation. VitC enhances epigenetic modifications, including DNA and histone demethylation, and promotes cell reprogramming (Esteban

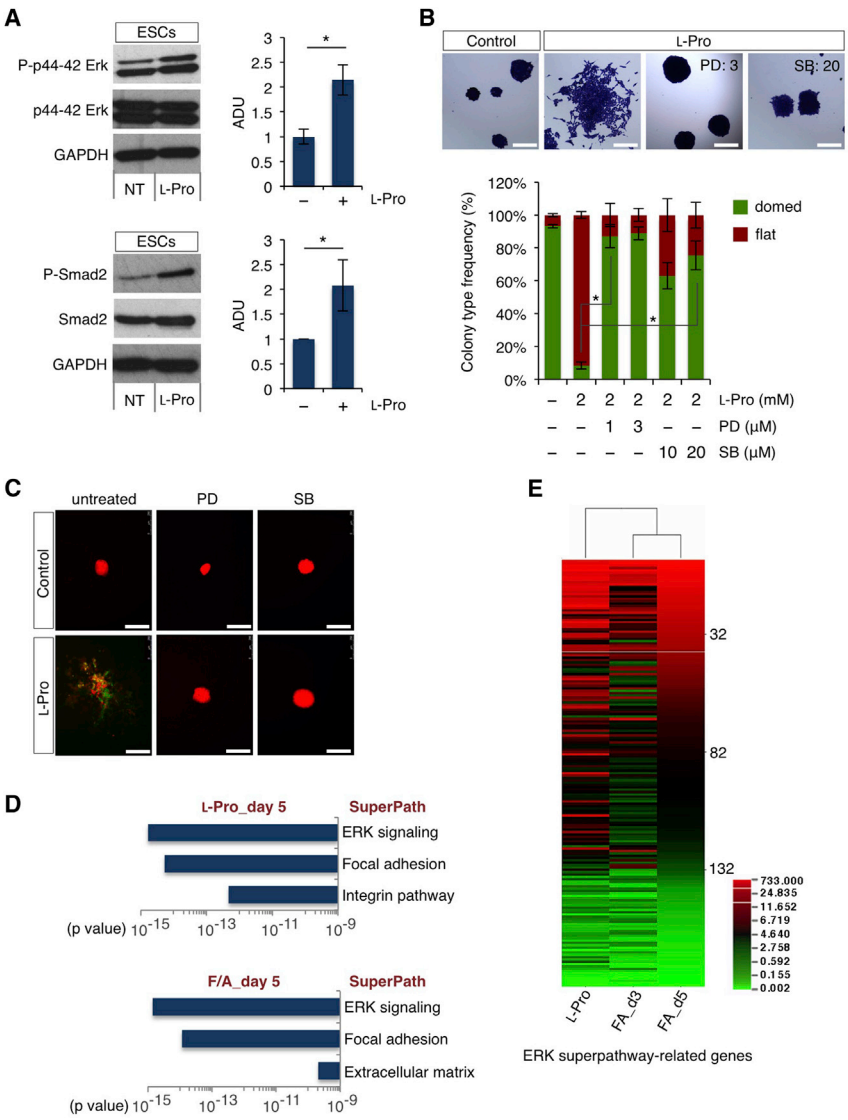

Figure 4. L-Proline Induces FGF and TGF-β Signaling in ESCs

(A) Western blot analysis of phospho-Erk/Erk (upper panels) and phospho-Smad2/Smad2 proteins (lower panels) in ESCs ± L-Pro (1 mM; 20 hr). Anti-Gapdh antibody was used as loading control. Densitometric analysis (ADU) is shown as pErk/Erk and pSmad2/Smad2 ratio. Data are mean ± SEM; *$p < 0.05$ ($n = 3$ independent experiments).

(B) Representative photomicrographs (upper panels) of colonies generated from ESCs ± L-Pro, either alone or ±PD0325901 (PD, 1–3 μM) or SB431542 (SB, 10–20 μM), and stained with crystal violet. Scale bars, 250 μm. Classification of colonies based on their morphology (lower panel). Data are mean ± SEM; *$p < 0.01$ ($n = 3$ independent experiments).

(C) Representative images of mCherry$^+$ colonies generated from ESCs ± L-Pro (1 mM), either alone or ±PD or SB, at day 5. Scale bars, 250 μm.

(D) Transcriptome analysis using GeneAnalytics software showing the enrichment in Erk pathway-associated genes in L-Pro- and FA-treated cells (day 5).

(E) Heatmap showing Erk-superpathway-related genes deregulated in L-Pro-treated (day 5) and F/A-treated (days 3 and 5) ESCs. See also Figure S3.

et al., 2010; Stadtfeld et al., 2012; Wang et al., 2011). Here we show that VitC and L-Pro supplementation oppositely modify DNA methylation at genomic regions that normally gain methylation during the blastocyst to epiblast transition (Blaschke et al., 2013). The DNA demethylation effect of VitC is well explained by its ability to positively regulate Fe(II)/oxoglutarate-dependent dioxygenase enzymes of the TET family (5mC to 5hmC conversion) (Blaschke et al., 2013; von Meyenn et al., 2016). Conversely, no data have been reported so far linking L-Pro and DNA methylation. Although the molecular mechanism by which a sudden increase of L-Pro induces DNA methylation in ESCs is still far from being fully elucidated, we suggest that L-Pro may influence VitC homeostasis, reducing its availability/activity for the TET demethylases. First, the vast majority of the genomic regions that are hypomethylated in VitC-treated ESCs are in turn hypermethylated upon L-Pro supplementation. Moreover, at appropriate stoichiometric ratios, VitC fully counteracts L-Pro-induced DNA methylation. How may L-Pro affect VitC availability? L-Pro could alter the redox balance and eventually induce VitC oxidation, i.e., its conversion to dehydroascorbic acid, by generating reactive oxygen species, which are by-product of the activity of mitochondrial L-Pro oxidase enzyme (PRODH/POX) (Phang et al., 2010). However, previous findings argue against a primary role of oxidative stress/redox signaling in this process (Comes et al., 2013; D'Aniello et al., 2015), and further evidence comes from metabolomics analysis, which reveals no sign of global oxidation and even higher levels of reduced glutathione (GSH) in L-Pro-treated cells (Figure 3G and Table S4), suggesting that L-Pro supplementation does not exert an

oxidizing effect in these culture conditions. Thus, we propose that the mechanism by which VitC and L-Pro antagonistic effects capture alternative states in the pluripotency continuum does not rely, at least primarily, on altered redox balance, which would favor a reducing (VitC) versus an oxidant (L-Pro) state. Of note, this is consistent with the idea that pluripotency is linked to a reduced state, while activation of oxidation is a metabolic signature of ESC differentiation (Yanes et al., 2010). Indeed, the GSH/glutathione disulfide (GSSG) ratio and VitC levels are inversely correlated in ESC cardiac and neural differentiation, suggesting that VitC compensates for GSSG accumulation to maintain homeostasis (Yanes et al., 2010). Since L-Pro activity depends on protein synthesis (D'Aniello et al., 2015), we hypothesize that a sudden increase of L-Pro could influence VitC homeostasis/availability, at least in part, by inducing the synthesis of L-Pro-rich proteins such as collagens. Indeed, nascent collagens are modified by VitC-dependent Fe(II)/oxoglutarate-dependent prolyl hydroxylase enzymes (Gorres and Raines, 2010). Thus, an abrupt increment of collagen biosynthesis/hydroxylation may reduce VitC availability for TET demethylases as well as for other VitC-dependent enzymes, such as the prolyl hydroxylases that regulate the hypoxia-inducible factor (HIF) steady-state level (Fong and Takeda, 2008). Interestingly, HIF is a key regulator of the metabolic reprogramming and is stabilized in primed but not in naive human ESCs (Sperber et al., 2015; Zhou et al., 2012). Of note, some of the HIF targets are induced in L-Pro-treated cells, such as *Ldha*, *Pfkfb3*, *Plin2*, *Gbe1*, and *Pygl* (Table S2). Although future studies are needed to clarify the molecular mechanisms, our findings have important implications for stem cell biology as they provide insights into how the availability of natural metabolites contribute to global epigenetic changes regulating alternative pluripotent states (Carey et al., 2015; Ryall et al., 2015; Wang et al., 2009). Furthermore, they attest to the definition of the optimal culture conditions for the capture in vitro of an early primed state of pluripotency.

EXPERIMENTAL PROCEDURES

Full details of the Experimental Procedure are included in Supplemental Experimental Procedures.

Culture of ESCs, Reagents, and Treatments

Wild-type TBV2 (129/SvP) and dual-reporter (DRESCs) mouse ESCs were maintained on a feeder layer of mitomycin C-treated MEFs according to standard procedures. ESC to PiC transition and ESC to EpiSC transition were performed as previously described (Casalino et al., 2011; Guo et al., 2009).

VitC was dissolved in water and used at the indicated concentrations (100–500 μM). VitC/L-Pro were added concomitantly. PD0325901 and SB431542 (Sigma-Aldrich) were used at concentration ranging from 1 to 3 μM and 10 to 20 μM, respectively. 2-Deoxy-D-glucose (2-DG, Sigma-Aldrich) was dissolved in water and used at concentration ranging from 6.25 to 50 mM.

5mC and 5hmC HPLC-MS/MS Measurement

Genomic DNA was extracted using the Wizard Genomic DNA Purification kit (Promega). 5mC and 5hmC high-performance liquid chromatography (HPLC)-tandem MS measurements were performed as described previously (Kroeze et al., 2014).

RNA Sequencing and Reduced Representation Bisulfite Sequencing

RNA sequencing and RRBS were performed at the Institute of Applied Genomics (Udine, Italy).

NMR-Based Metabolomic Analysis

The metabolic profiles were acquired through NMR spectroscopy. Details on data processing are provided in Supplemental Experimental Procedures.

Statistical Analysis

Statistical significance was determined by a two-tailed paired Student's t test. p Values of <0.05 were considered as statistically significant. Error bars in the figures represent SEM.

Multivariate statistical analysis of NMR data was performed using SIMCA 14 software (Umetrics). Details are provided in Supplemental Experimental Procedures.

ACCESSION NUMBERS

The accession number for all RNAseq and RRBS data reported in this paper is GEO: GSE84373.

SUPPLEMENTAL INFORMATION

Supplemental Information includes Supplemental Experimental Procedures, three figures, and six tables and can be found with this article online at http://dx.doi.org/10.1016/j.stemcr.2016.11.011.

AUTHOR CONTRIBUTIONS

C.D'A., A.F., D.d.C., E.J.P., and G.M. conceived and designed the study. C.D'A., D.d.C., F.C., G.d.N., A.F., E.H., and G.C. performed the experiments. E.H., F.R., and C.A. performed bioinformatics analysis. D.P., D.J.M., and A.M. performed metabolomics analysis. R.B., A.M., and H.G.S. gave conceptual advice and edited the manuscript. C.D'A., E.J.P., and G.M. wrote the manuscript.

ACKNOWLEDGMENTS

We are grateful to members of the Integrated Microscopy and FACS Facilities of IGB-ABT, CNR. We thank Gennaro Andolfi for excellent technical assistance. This study was supported by Epigenomics Flagship Project (EPIGEN) MIUR-CNR to G.M. and C.A., and AIRC (grant 11599), Italian Ministry of Education-University-Research (grant CTN01_00177 Cluster ALISEI_IRMI and PRIN) and CARIPLO to G.M.

Received: April 12, 2016
Revised: November 24, 2016
Accepted: November 25, 2016
Published: December 22, 2016

REFERENCES

Blaschke, K., Ebata, K.T., Karimi, M.M., Zepeda-Martinez, J.A., Goyal, P., Mahapatra, S., Tam, A., Laird, D.J., Hirst, M., Rao, A., et al. (2013). Vitamin C induces Tet-dependent DNA demethylation and a blastocyst-like state in ES cells. Nature *500*, 222–226.

Carey, B.W., Finley, L.W., Cross, J.R., Allis, C.D., and Thompson, C.B. (2015). Intracellular alpha-ketoglutarate maintains the pluripotency of embryonic stem cells. Nature *518*, 413–416.

Casalino, L., Comes, S., Lambazzi, G., De Stefano, B., Filosa, S., De Falco, S., De Cesare, D., Minchiotti, G., and Patriarca, E.J. (2011). Control of embryonic stem cell metastability by L-proline catabolism. J. Mol. Cell Biol. *3*, 108–122.

Comes, S., Gagliardi, M., Laprano, N., Fico, A., Cimmino, A., Palamidessi, A., De Cesare, D., De Falco, S., Angelini, C., Scita, G., et al. (2013). L-Proline induces a mesenchymal-like invasive program in embryonic stem cells by remodeling H3K9 and H3K36 methylation. Stem Cell Reports *1*, 307–321.

D'Aniello, C., Fico, A., Casalino, L., Guardiola, O., Di Napoli, G., Cermola, F., De Cesare, D., Tate, R., Cobellis, G., Patriarca, E.J., et al. (2015). A novel autoregulatory loop between the Gcn2-Atf4 pathway and (L)-Proline [corrected] metabolism controls stem cell identity. Cell Death Differ. *22*, 1094–1105.

Esteban, M.A., Wang, T., Qin, B., Yang, J., Qin, D., Cai, J., Li, W., Weng, Z., Chen, J., Ni, S., et al. (2010). Vitamin C enhances the generation of mouse and human induced pluripotent stem cells. Cell Stem Cell *6*, 71–79.

Fico, A., Manganelli, G., Simeone, M., Guido, S., Minchiotti, G., and Filosa, S. (2008). High-throughput screening-compatible single-step protocol to differentiate embryonic stem cells in neurons. Stem Cell Dev. *17*, 573–584.

Fong, G.H., and Takeda, K. (2008). Role and regulation of prolyl hydroxylase domain proteins. Cell Death Differ. *15*, 635–641.

Gorres, K.L., and Raines, R.T. (2010). Prolyl 4-hydroxylase. Crit. Rev. Biochem. Mol. Biol. *45*, 106–124.

Guo, G., Yang, J., Nichols, J., Hall, J.S., Eyres, I., Mansfield, W., and Smith, A. (2009). Klf4 reverts developmentally programmed restriction of ground state pluripotency. Development *136*, 1063–1069.

Habibi, E., Brinkman, A.B., Arand, J., Kroeze, L.I., Kerstens, H.H., Matarese, F., Lepikhov, K., Gut, M., Brun-Heath, I., Hubner, N.C., et al. (2013). Whole-genome bisulfite sequencing of two distinct interconvertible DNA methylomes of mouse embryonic stem cells. Cell Stem Cell *13*, 360–369.

Hackett, J.A., and Surani, M.A. (2014). Regulatory principles of pluripotency: from the ground state up. Cell Stem Cell *15*, 416–430.

Harvey, A.J., Rathjen, J., and Gardner, D.K. (2016). Metaboloepigenetic regulation of pluripotent stem cells. Stem Cell Int. *2016*, 1816525.

Hayashi, K., Lopes, S.M., Tang, F., and Surani, M.A. (2008). Dynamic equilibrium and heterogeneity of mouse pluripotent stem cells with distinct functional and epigenetic states. Cell Stem Cell *3*, 391–401.

Hore, T.A., von Meyenn, F., Ravichandran, M., Bachman, M., Ficz, G., Oxley, D., Santos, F., Balasubramanian, S., Jurkowski, T.P., and Reik, W. (2016). Retinol and ascorbate drive erasure of epigenetic memory and enhance reprogramming to naive pluripotency by complementary mechanisms. Proc. Natl. Acad. Sci. USA *113*, 12202–12207.

Krishnakumar, R., and Blelloch, R.H. (2013). Epigenetics of cellular reprogramming. Curr. Opin. Genet. Dev. *23*, 548–555.

Kroeze, L.I., Aslanyan, M.G., van Rooij, A., Koorenhof-Scheele, T.N., Massop, M., Carell, T., Boezeman, J.B., Marie, J.P., Halkes, C.J., de Witte, T., et al. (2014). Characterization of acute myeloid leukemia based on levels of global hydroxymethylation. Blood *124*, 1110–1118.

Martello, G., and Smith, A. (2014). The nature of embryonic stem cells. Annu. Rev. Cell Dev. Biol. *30*, 647–675.

Martinez Arias, A., Nichols, J., and Schroter, C. (2013). A molecular basis for developmental plasticity in early mammalian embryos. Development *140*, 3499–3510.

Maruotti, J., Dai, X.P., Brochard, V., Jouneau, L., Liu, J., Bonnet-Garnier, A., Jammes, H., Vallier, L., Brons, I.G., Pedersen, R., et al. (2010). Nuclear transfer-derived epiblast stem cells are transcriptionally and epigenetically distinguishable from their fertilized-derived counterparts. Stem Cells *28*, 743–752.

Monfort, A., and Wutz, A. (2013). Breathing-in epigenetic change with vitamin C. EMBO Rep. *14*, 337–346.

Parchem, R.J., Ye, J., Judson, R.L., LaRussa, M.F., Krishnakumar, R., Blelloch, A., Oldham, M.C., and Blelloch, R. (2014). Two miRNA clusters reveal alternative paths in late-stage reprogramming. Cell Stem Cell *14*, 617–631.

Phang, J.M., Liu, W., and Zabirnyk, O. (2010). Proline metabolism and microenvironmental stress. Annu. Rev. Nutr. *30*, 441–463.

Ryall, J.G., Cliff, T., Dalton, S., and Sartorelli, V. (2015). Metabolic reprogramming of stem cell epigenetics. Cell Stem Cell *17*, 651–662.

Shyh-Chang, N., Locasale, J.W., Lyssiotis, C.A., Zheng, Y., Teo, R.Y., Ratanasirintrawoot, S., Zhang, J., Onder, T., Unternaehrer, J.J., Zhu, H., et al. (2012). Influence of threonine metabolism on S-adenosylmethionine and histone methylation. Science *339*, 222–226.

Sperber, H., Mathieu, J., Wang, Y., Ferreccio, A., Hesson, J., Xu, Z., Fischer, K.A., Devi, A., Detraux, D., Gu, H., et al. (2015). The metabolome regulates the epigenetic landscape during naive-to-primed human embryonic stem cell transition. Nat. Cell Biol. *17*, 1523–1535.

Stadtfeld, M., Apostolou, E., Ferrari, F., Choi, J., Walsh, R.M., Chen, T., Ooi, S.S., Kim, S.Y., Bestor, T.H., Shioda, T., et al. (2012). Ascorbic acid prevents loss of Dlk1-Dio3 imprinting and facilitates generation of all-iPS cell mice from terminally differentiated B cells. Nat. Genet. *44*, 398–405, S1–2.

Tesar, P.J. (2016). Snapshots of pluripotency. Stem Cell Reports *6*, 163–167.

Toyooka, Y., Shimosato, D., Murakami, K., Takahashi, K., and Niwa, H. (2008). Identification and characterization of subpopulations in undifferentiated ES cell culture. Development *135*, 909–918.

von Meyenn, F., Iurlaro, M., Habibi, E., Liu, N.Q., Salehzadeh-Yazdi, A., Santos, F., Petrini, E., Milagre, I., Yu, M., Xie, Z., et al. (2016). Impairment of DNA methylation maintenance is the main cause of global demethylation in naive embryonic stem cells. Mol. Cell *62*, 848–861.

Wang, J., Alexander, P., Wu, L., Hammer, R., Cleaver, O., and McKnight, S.L. (2009). Dependence of mouse embryonic stem cells on threonine catabolism. Science *325*, 435–439.

Wang, T., Chen, K., Zeng, X., Yang, J., Wu, Y., Shi, X., Qin, B., Zeng, L., Esteban, M.A., Pan, G., et al. (2011). The histone demethylases Jhdm1a/1b enhance somatic cell reprogramming in a vitamin-C-dependent manner. Cell Stem Cell *9*, 575–587.

Washington, J.M., Rathjen, J., Felquer, F., Lonic, A., Bettess, M.D., Hamra, N., Semendric, L., Tan, B.S., Lake, J.A., Keough, R.A., et al. (2010). L-Proline induces differentiation of ES cells: a novel role for an amino acid in the regulation of pluripotent cells in culture. Am. J. Physiol. Cell Physiol. *298*, C982–C992.

Weinberger, L., Ayyash, M., Novershtern, N., and Hanna, J.H. (2016). Dynamic stem cell states: naive to primed pluripotency in rodents and humans. Nat. Rev. Mol. Cell Biol. *17*, 155–169.

Wu, J., and Izpisua Belmonte, J.C. (2015). Dynamic pluripotent stem cell states and their applications. Cell Stem Cell *17*, 509–525.

Yanes, O., Clark, J., Wong, D.M., Patti, G.J., Sanchez-Ruiz, A., Benton, H.P., Trauger, S.A., Desponts, C., Ding, S., and Siuzdak, G. (2010). Metabolic oxidation regulates embryonic stem cell differentiation. Nat. Chem. Biol. *6*, 411–417.

Zhou, W., Choi, M., Margineantu, D., Margaretha, L., Hesson, J., Cavanaugh, C., Blau, C.A., Horwitz, M.S., Hockenbery, D., Ware, C., et al. (2012). HIF1alpha induced switch from bivalent to exclusively glycolytic metabolism during ESC-to-EpiSC/hESC transition. EMBO J. *31*, 2103–2116.

Stem Cell Reports, Volume *8*

Supplemental Information

Vitamin C and L-Proline Antagonistic Effects Capture Alternative States in the Pluripotency Continuum

Cristina D'Aniello, Ehsan Habibi, Federica Cermola, Debora Paris, Francesco Russo, Alessandro Fiorenzano, Gabriele Di Napoli, Dominique J. Melck, Gilda Cobellis, Claudia Angelini, Annalisa Fico, Robert Blelloch, Andrea Motta, Hendrik G. Stunnenberg, Dario De Cesare, Eduardo J. Patriarca, and Gabriella Minchiotti

SUPPLEMENTAL INFORMATION

Document S1. Figures S1-S3, Tables S1-S6 and Supplemental Experimental Procedures

Supplemental Figures

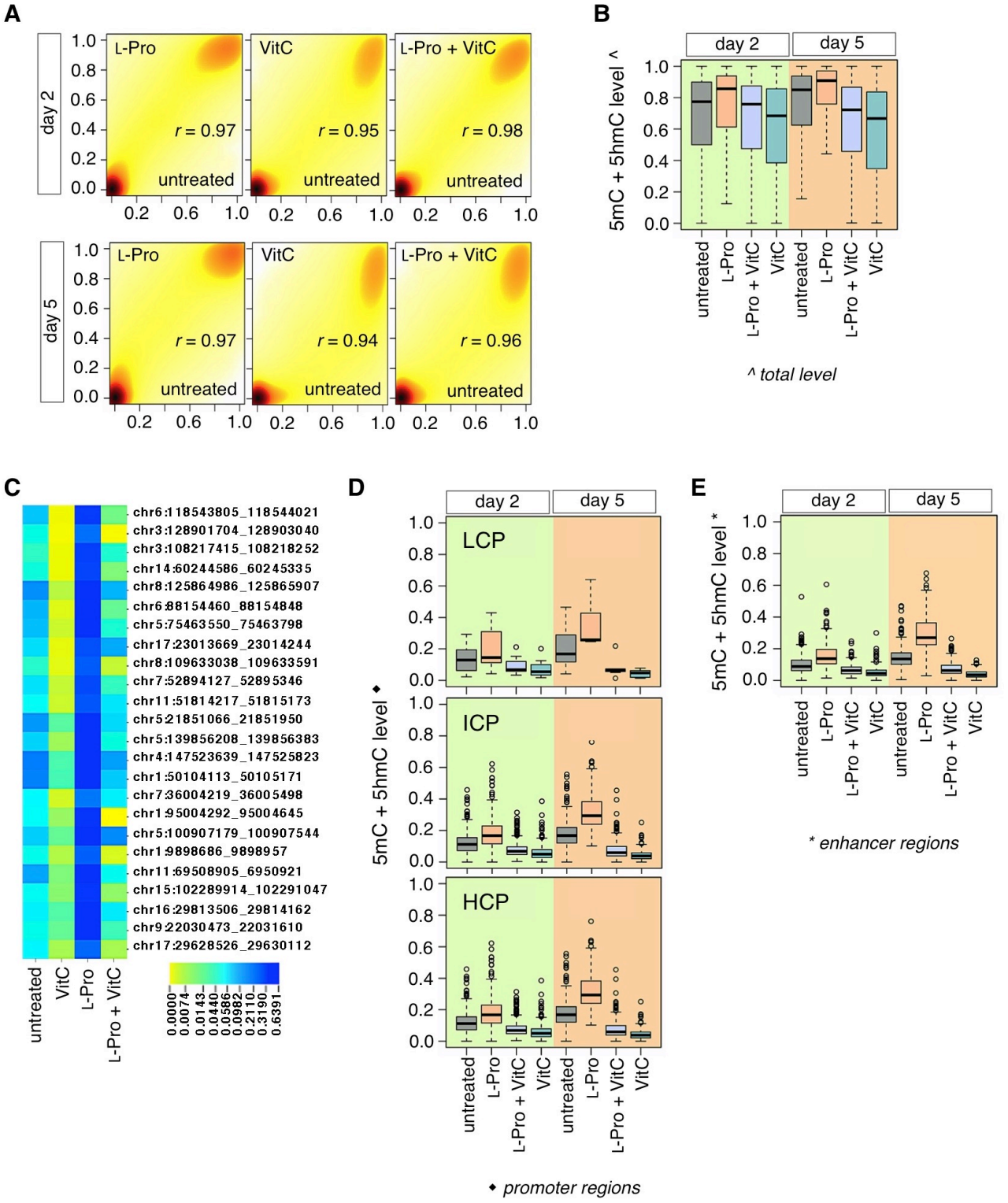

Figure S1. Effect of Vitamin C and L-Proline on DNA Methylation (related to Figure 1)

(A) Density scatterplot of mean methylation levels of the sliding windows. The Pearson correlation coefficients between the different conditions were high ($r > 0.94$).

(B) Global methylation levels in ESCs treated with VitC (500 µM) and L-Pro (150 µM), either alone or in combination, at day 2 and 5 or left untreated as control.

(C) Heatmap (CIMminer, http://discover.nci.nih.gov/cimminer/) showing the methylation levels at 24 selected loci in ESCs ± VitC (500 µM) and ± L-Pro (150 µM) at day 5.

(D) Average profile of methylation over low CpG density promoters (LCP), Intermediate (ICP) and High (HCP).

(E) Average profile of methylation over enhancers.

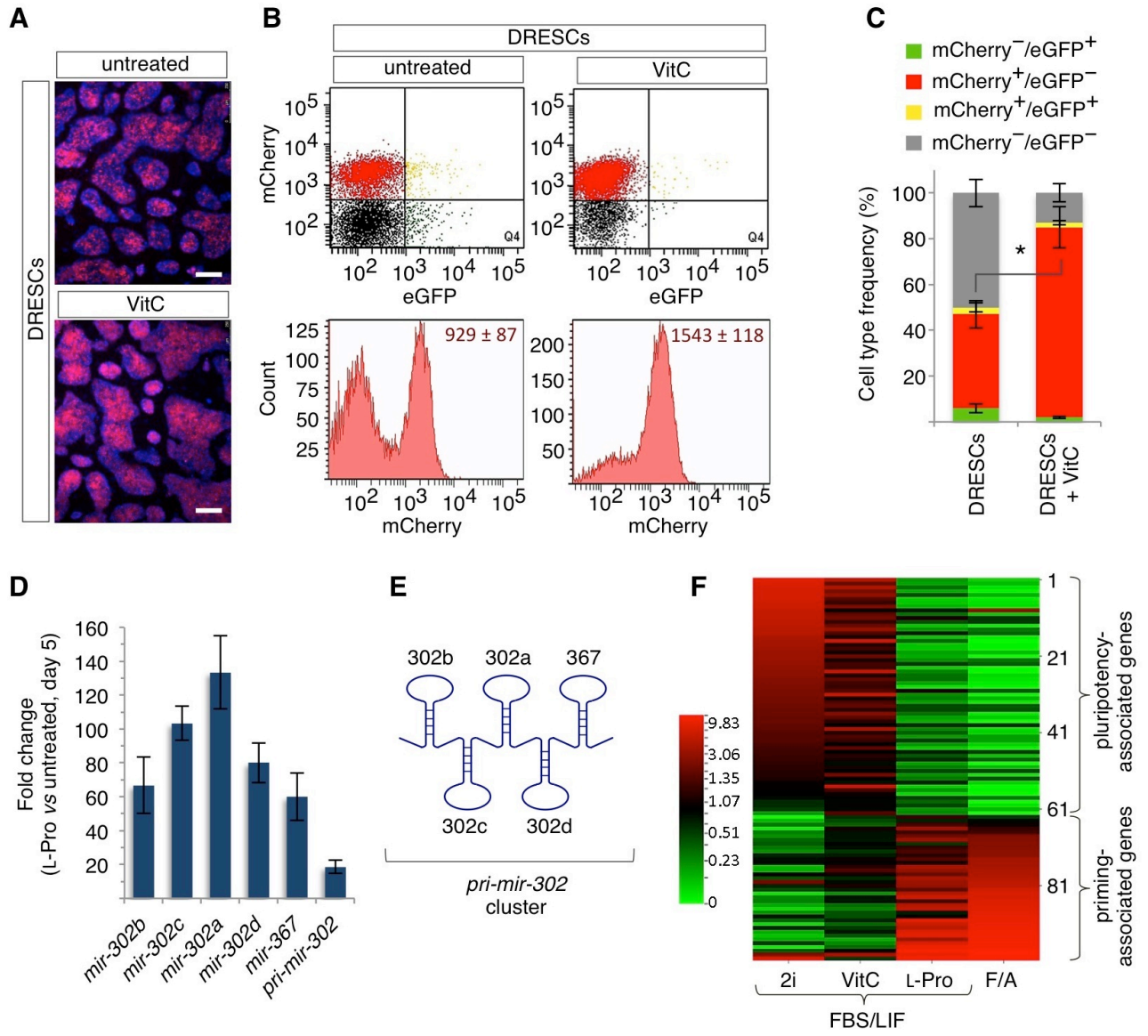

Figure S2. Effect of Vitamin C and L-Proline on *mir-290* and *mir-302* Expression (related to Figure 2)

(A) Representative fluorescence images of DRESCs grown on a feeder layer, in the presence or absence of VitC (100 µM) for three passages. Scale bar, 125 µm.

(B) Representative FACS plots showing the percentage of mCherry±/eGFP± cells (*upper panels*) and mCherry intensity mean (*lower panels*) in untreated and VitC- treated (100 µM) DRESCs.

(C) Quantification of mCherry±/eGFP± cells in DRESCs ± VitC (100 µM). Data are mean ± SEM, *p < 0.001 (n = 3 independent experiments).

(D) qPCR analysis of *mir-302* family members' expression in ESCs treated with L-Pro (1 mM) for 5 days. Data are fold change *versus* control (- L-Pro) after normalization to *Gapdh* and are mean ± SEM (n = 3 independent experiments).

(E) Schematic representation of *mir-302* cluster, including *mir-302b*, *c*, *a*, *d* and the *mir-367* members (*pri-mir-302/367*).

(F) Heatmap (CIMminer, http://discover.nci.nih.gov/cimminer/) showing pluripotency and priming associated genes in ESCs grown in FBS/LIF + 2i, VitC, −− (untreated), L-Pro or F/A.

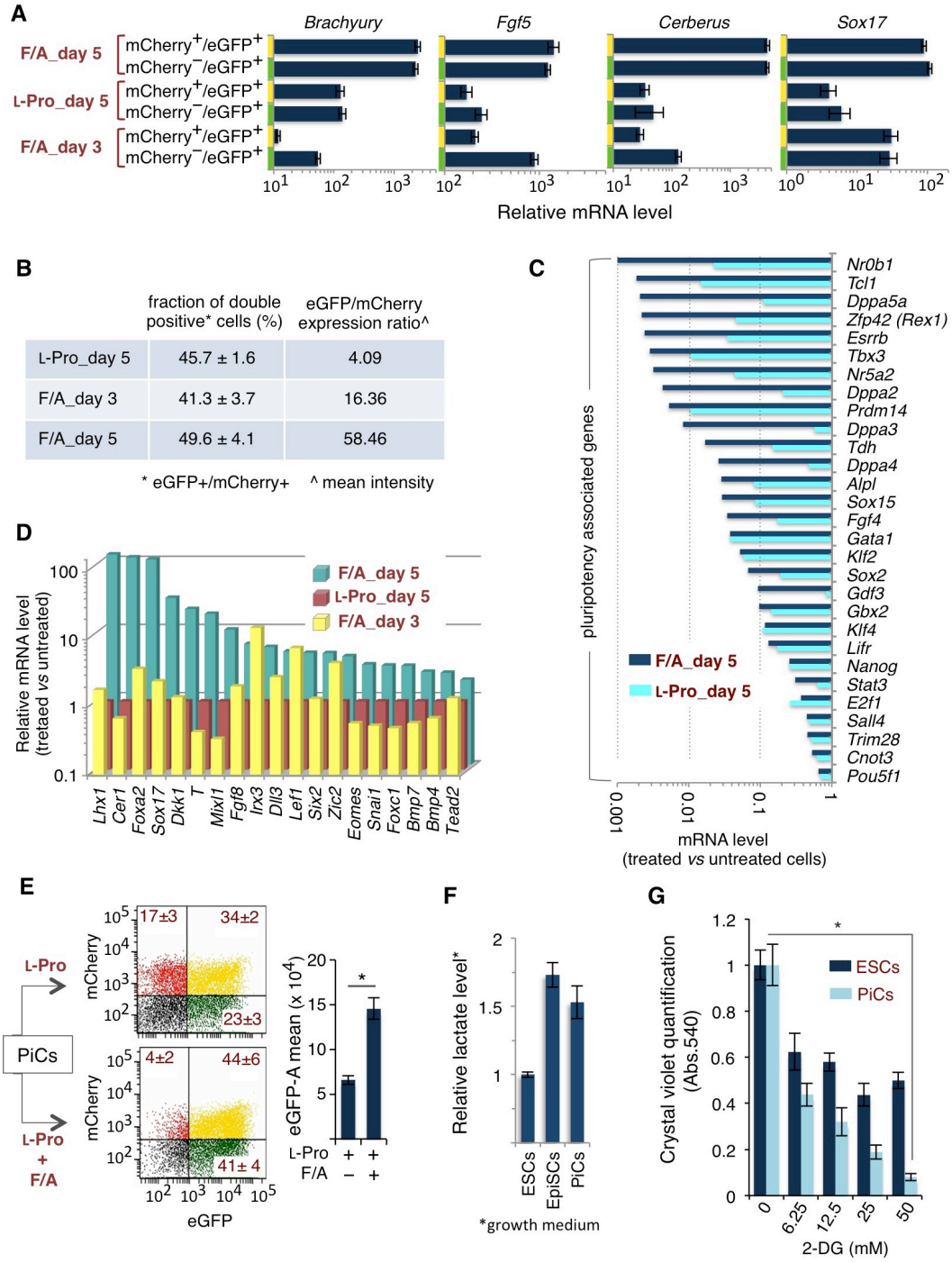

Figure S3. Effect of bFgf/Activin A and L-Proline on ESC Transcription Profile and on the Distribution of mCherry±/eGFP± Cells (related to Figure 3)

(A) qPCR gene expression analysis in mCherry±/eGFP+ cells derived from L-Pro- (day 5) and F/A- (day 3 and 5) treated DRESCs. mRNA levels were normalized to *Gapdh*. Data are mean ± SEM (n = 3 independent experiments).

(B) Fraction of mCherry+eGFP+ cells and eGFP/mCherry ratio in L-Pro- (day 5) and F/A- (day 3 and 5) treated cells. Data are mean ± SEM (n = 3 independent experiments).

(C) mRNA levels of pluripotency associated genes in L-Pro- and F/A- treated cells (day 5) *versus* untreated cells.

(D) mRNA levels of a set of mesendodermal genes in L-Pro- (day 5) and F/A- (day 3 and 5) treated cells.

(E) Representative FACS plots showing the percentage of mCherry±/eGFP± cells (*left panels*) and eGFP intensity mean (*right panels*) in L-Pro- induced cells (PiCs) treated with either L-Pro or L-Pro/F/A for further 3 days. Data are mean ± SEM, *p < 0.01 (n = 3 independent experiments).

(F) Lactate level measured in the conditioned medium derived from ESCs, F/A-EpiSCs and L-Pro -induced cells (PiCs). Data are shown as fold change *versus* ESCs and are mean ± SEM (n = 3 independent experiments).

(G) Dose-dependent effect of the glycolysis inhibitor 2-DG. Quantification of crystal violet staining of ESCs and L-Pro -induced cells (PiCs) at day 5 treated with the glycolysis inhibitor 2-DG (6.25-50 mM, for 16 hours) or left untreated as

control. Data are mean ± SEM (n = 3 independent experiments).

Supplemental Tables

Table S1. List of Differentially Methylated Regions (DMRs); Genes whose Promoters are Differentially Methylated; DMRs- Associated Genes in L-Pro- and VitC- Treated ESCs, Related to Figure 1.
Table S2. List of Differentially Expressed Genes and of Pluripotency-Associated and Priming Markers in 2i-, VitC-, Untreated, L-Pro- and F/A- Treated cells, Related to Figure 2.
Table S3. List of Differentially Expressed Genes; Genes Related to Pluripotency, Mesendodermal Specification, and ERK Superpathway Differentially Expressed in F/A- and L-Pro- Treated Cells, Related to Figure 3.
Table S4. List of Metabolites Deregulated by Supplemental L-Pro in ESCs, Related to Figure 3 and Discussion.
Table S5. Pluripotency-Associated Properties in ESCs, PiCs and EpiSCs, Related to Discussion.
Table S6. Primer Sequences for mRNA/miRNA and qPCR Analysis, Related to Experimental Procedures.

Table S4. List of Metabolites Deregulated by Supplemental L-Pro in ESCs. Relevant metabolites, as found by NMR-based metabolomics, (Variable Importance in Projection (VIP) > 1 and |pcorr| > 0.66) and the chemical shift of the buckets (the isolated variables selected for quantification) are shown. Values are fold-change ratio (L-Pro- treated *vs.* untreated cells) ± standard deviation of the NMR variables normalized to the total area of the spectrum, Related to Figure 3 and Discussion.

Metabolites	Chemical shift (ppm)	Fold change (PiCs vs ESCs)
Taurine	[3.39-3.41]	1.57±0.59
Proline	[3.33-3.35]	1.51±0.13
Lactate	[4.13-4.15]	1.47±0.14
Glycerol	[3.65-3.67]	1.37±0.13
GSH	[2.55-2.57]	1.37±0.24
Glutamate	[2.33-2.35]	1.34±0.21
Phosphocholine	[3.21-3.23]	1.24±0.13
Gaba	[2.25-2.27]	1.23±0.13
UDP-N-AcetylGlucosamine	[7.95-7.97]	-1.26±0.15
Serine	[3.95-3.97]	-1.28±0.23
Leucine	[0.95-0.97]	-1.34±0.35
AMP	[8.59-8.61]	-1.43±0.19
Valine	[0.99-1.01]	-1.29±0.31
Alanine	[1.47-1.49]	-1.73±0.34
Glycine	[3.55-3.57]	-1.99±0.28
Tyrosine	[6.87-6.89]	-1.98±0.76
Glutamine	[2.43-2.45]	-2.19±0.56

Table S5. Pluripotency-Associated Properties in ESCs, PiCs and EpiSCs, Related to Discussion.

Pluripotency-associated property	**ESCs (naïve)**	**PiCs (early-primed)**	**EpiSCs (primed)**
MEK_ERK activation	No	Yes	Yes
Tgfβ-ActivinA activation	No	Yes	Yes
Global DNA hypomethylation	Yes	No	No
Pluripotency markers	↑	↓	↓↓
Priming markers	↓	↑	↑↑
Adhesion molecules	E-Cadherin	N-Cadherin	N-Cadherin
Sensibility to Trypsin	No	Yes	Yes
Metabolism	OxPhos/Glycolytic	Glycolytic	Glycolytic
Contribution to chimeric embryos	High	High	Low

Table S6. Primer Sequences for mRNA/miRNA and qPCR Analysis, Related to Experimental Procedures.

Primer sequences for miRNA qPCR analysis

Primer	Target Sequence	Exiqon product no.
hsa-mir-302a-3p	UAAGUGCUUCCAUGUUUUGGUGA	206059
hsa-mir-302b-3p	UAAGUGCUUCCAUGUUUUAGUAG	204773
hsa-mir-302c-3p	UAAGUGCUUCCAUGUUUCAGUGG	204403
hsa-mir-302d-3p	UAAGUGCUUCCAUGUUUGAGUGU	204311
hsa-mir -367-3p	AAUUGCACUUUAGCAAUGGUGA	204784
mmu-mir -293-3p	AGUGCCGCAGAGUUUGUAGUGU	205003
mmu-mir -294-3p	AAAGUGCUUCCCUUUUGUGUGU	205166
mmu-mir -293-3p	AAAGUGCUACUACUUUUGAGUCU	205078

Primer sequences for qPCR analysis

Primer	Forward	Reverse
pri-mir-302	CTGTGGGTTTGCTCTTCTGTTTT	GAGACAGAAAGCATTCCCATGTT
Fgf5	CAAAGTCAATGGCTCCCACGAAG	CTACAATCCCCTGAGACACAGCAAATA
Pitx2	AGCTGTGCAAGAATGGCTTT	CACCATGCTGGACGACATAC
Inhbb	CGAGATCATCAGCTTTGCAG	TGGTTGCCTTCATTAGAGACG
Brachyury (T)	GAACCTCGGATTCACATCGTGAGA	ATCAAGGAAGGCTTTAGCAAATGGG
Cerberus	AGGAGGAAGCCAAGAGGTTC	CATTTGCCAAAGCAAAGGTT
Sox17	AGCTAAGCAAGATGCTAGGCAAG	TCTCTGCCAAGGTCAACGC
Gapdh	TGCACCACCAACTGCTTAGC	TCTTCTGGGTGGCAGTGATG

Supplemental Experimental Procedures

***In vitro* Generation of L-Proline- Induced Cells (PiCs) and Epiblast Stem Cells (EpiSCs) and Differentiation**

ESCs were cultured in high glucose Dulbecco's modified Eagle's medium (Invitrogen, Life Technologies) supplemented with 15% ES- screened fetal bovine serum (FBS, Euroclone) 0.1 mM β-mercaptoethanol (Sigma-Aldrich), 1 mM sodium pyruvate, 2 mM glutamine, 100 U/ml penicillin/streptomycin all from GIBCO and 1000 U/ml recombinant LIF (ESGRO, Millipore).

2i medium was supplemented with PD0325901 (1 μM) and CHIR99021 (3 μM).

To induce ESC to PiC transition, ESCs were seeded at low density (50–500 cells/cm^2) onto gelatin-coated plates and grown in ESC medium (described above) in the presence of L-Pro (from 500 μM to 2 mM) for 5 days. Medium was changed at day 3 with addition of fresh L-Pro. PiCs were harvested using accutase (Sigma-Aldrich) and cultured in the presence of L-Pro (500 μM).

For ESC to EpiSC transition, ESCs were plated at 1500 cells/cm^2 onto FBS- coated plates and grown in N2/B27 supplemented with 20 ng/ml Activin A (Invitrogen) and 12 ng/ml Fgf2 (Provitro) and cultured for 5 days. Cell colonies were washed twice with phosphate-buffered saline (PBS) and fixed/stained with a solution of 6% glutaraldehyde and crystal violet for 30 min at RT. Cells were carefully washed with tap water and dried for further analysis. For quantification, crystal violet was dissolved with 30% acetic acid for 15 min at RT and absorbance was read at 540 nm, using the Synergy H1 Microplate Reader (BioTek).

Alkaline phosphatase assay was performed using the AP staining kit (System Biosciences), following the manufacturer's instructions.

Neuronal differentiation was performed as previously described (Fico et al., 2008).

5mC and 5hmC HPLC-MS/MS Measurement

DNA degradase plus (ZymoResearch) was used to degrade 2 μg of DNA into individual nucleosides (dG, mdC and hmdC) that were measured using a high performance liquid chromatography-tandem mass spectrometry (HPLC-MS/MS) system. Calibration standards were used to obtain area-based linear regression curves for quantification. The 5mC and 5hmC levels are presented as a ratio of %mdC/dG and %hmdC/dG, respectively.

Flow Cytometry and Cell Sorting

ESCs, PiCs and EpiSCs were dissociated to obtain a single cell suspension, using trypsin-EDTA, and analysed/sorted on the basis of mCherry and eGFP signals, with a FACS Aria (Becton Dickinson). For evaluating oxidative phosphorylation, the TMRE Mitochondrial Membrane Potential Assay kit (Abcam) was used, using the manufacturer instructions.

RNA Extraction and Quantitative Real-Time PCR

Total RNAs were isolated using either the RNeasy kit or Trizol reagent (Invitrogen) and reverse transcribed using QuantiTect Reverse Transcription kit (Qiagen). For miRNA expression analysis, RNAs were reverse transcribed using miRCURY LNA Universal RT microRNA PCR kit (EXIQON), using the manufacturer instructions. qPCR was performed using SYBR Green PCR master mix (FluoCycle IITM SYBR, EuroClone). Primers for miRNAs were purchased from EXIQON and are listed in Table S6. Primers for the *pri-mir*-302 and the other genes were designed using Primer3 software and are listed in Table S6.

For RNA profiling 2 μg of extracted RNA was depleted from ribosomal RNA using Ribo-Zero Gold Kit (Epicentre Madison, Winsconsin, USA). Then, rRNA-depleted RNA was used for library preparation using the Kapa RNA Sample Prep Kit (Kapa Biosystems) following the manufacturer's instructions. Libraries were indexed using NEXTflex adapters (Bioo-Scientific Corporation, Austin, TX, USA) and 2 × 43 bp paired-end sequencing was performed on Illumina NextSeq 500 instruments using TruSeq reagents (Illumina, San Diego, CA, USA), according to manufacturer's instructions.

RNA Sequencing Analysis

For RNA-seq data analysis of FBS/LIF ± VitC, L-Pro, naïve/2i and F/A EpiSCs, raw data were aligned to the Mus musculus NCBIM37.67 (mm9) transcriptome using Bowtie 1 with the following setting: -a --best --strata -S -m 100 -X 500. Quantification of gene expression was performed using MMSEQ (Turro et al., 2011). The MMSEQ expression estimates are roughly in FPKM units (fragments per kilobase of transcript per million mapped reads or read pairs). To do the differential expression analysis, the raw counts were extracted from the MMSEQ outputs using the mmseq.R R script included in MMSEQ package. Next, the R package DESeq was used to normalize the data and then performed pair-wise comparisons (fold change 2, adjusted p-value <0.05 and FPKM>=1 in at least in any condition) to determine the differentially expressed genes per condition.

For RNA-seq data analysis of mCherry+/eGFP+ L-Pro- and F/A- induced cells, files were mapped against the reference genome (mm9, NCBI Build 37) http://hgdownload.cse.ucsc.edu/goldenPath/mm9/chromosomes/ and the transcript annotation Mus musculus.NCBIM37.67.gtf.gz (ftp://ftp.ensembl.org/pub/release-67/gtf/mus_musculus/ repository; version NCBIM37, release 67). For the mapping procedure, we run TopHat2 (Kim et al., 2013) by using the -G option to be guided by the annotation. We run htseq-count (version 0.6.1p1) (Anders et al., 2015) with the intersection-

nonempty mode in order to quantify the number of reads mapped on each gene. All the other analyses were performed by using RNASeqGUI (Russo and Angelini, 2014). Genes with low counts were filtered in all the samples by using the Filtering Proportional Test (Tarazona et al., 2011); this procedure reduced the number of genes from 37620 to 15441. 2. We then applied an Upper Quartile Normalization, and finally run NOISeq (version 2.10.0) (Tarazona et al., 2011) on the filtered and upperquartile- normalized count files. We considered a gene as differentially expressed across the samples if the posterior probability was greater or equal to 0.99 for NOISeq.

Reduced Representation Bisulfite Sequencing (RRBS)
FASTQ files were mapped against mm9 with BSMAP v2.88 using the parameters -R -v 0.1 -u -n 1 -s 12 -w 100 -D C-CGG -q 2. We extracted methylation levels per individual C as #C/(#C+#T) with methratio.py from BSMAP v2.88 using the parameters -z -u -g. For further analysis we filtered CGs to have a minimum sequencing depth of 10X.

Preparation of Cytospin Samples
Cells (1-1.5 x 10^4) were dissociated with accutase for 5 min at 37°C, resuspended in 15% FBS/1x PBS and centrifuged at 900 rpm for 15 min onto glass slides (2 spots of $1x10^5$ cells each) using a Thermo Shandon Cytocentrifuge (CytoSpin™ 4). Specimens were fixed for further analysis.

Immunofluorescence Analysis
Cells were fixed (4% PFA) and permeabilized (0.1% Triton X-100) for 10 minutes at RT and incubated with anti-Gfap (1:300, DAKO #Z0334) and βIII-Tubulin (1:400, SIGMA #T8660) antibodies overnight at 4°C. After washing in 0,5% Tween-1x PBS, cells were incubated with the appropriate secondary antibodies (Alexa Fluor DAR-594, 1:200, Molecular Probes #A21207; Alexa Fluor GAM-488, 1:200, Molecular Probes #A11001). Cell nuclei were counterstained with DAPI (Invitrogen). Images were obtained using the DMI6000B microscope and the DFC 350FX B/W digital camera (Leica). Leica FW4000 and AF6000 software were used for image acquisition/elaboration.

Western Blotting
Whole-cell lysates were prepared in 100 mM Tris pH 8, 140 mM NaCl, 20 mM EDTA, 0,2% SDS, 1% Nonidet P-40 lysis buffer, resolved on SDS-PAGE gels and transferred onto PVDF membranes using the iBlot dry Transfer System (Life Technologies). Blocked membranes were incubated with the following primary antibodies: phospho-Erk1/2 (1:1000, Cell Signaling #9101); Erk (1:1000, Cell Signaling #9102); phospho-Smad2 (1:200, Cell Signaling #3108); Smad2 (1:1000, Cell Signaling #3103); anti Gapdh (1:10000, Abcam #Ab8245), followed by the appropriate HRP-conjugated secondary antibodies (1:10000, GAM-HRP #P0447 and GAR-HRP #P0448 DAKO). Detection was performed with ECL reagents (Pierce, Thermo Scientific). For densitometric analysis the ImageJ software was used.

NMR-based Metabolomic Analysis
Cells extracts and NMR samples were prepared as described (Lindon et al., 2005). NMR spectra of polar extracts were recorded at 600.13 MHz on a Bruker Avance-600 spectrometer equipped with a TCI CryoProbe™ fitted with a gradient along the Z-axis, at a probe temperature of 300 K. Assignment of NMR signals to specific metabolites was obtained by homonuclear and heteronuclear 2D experiments (TOCSY to identify ^{1}H-^{1}H connectivities, and ^{1}H-^{13}C HSQC for directly bonded ^{1}H and ^{13}C nuclei). Assignments were also compared with literature data and/or online database (Wishart et al., 2007).

Multivariate Statistical Analysis
The 1D spectra, representing the metabolic profiles, were subjected to multivariate statistical analysis to identify trends and clusters (Eriksson et al., 2001). The statistical analysis projects NMR data into a lower dimensional space, where sample clustering based on similarities of biochemical profiles can be determined and easily visualized through scores plot. To that purpose, ^{1}H-NMR spectra were automatically data reduced to 440 integrated regions ("buckets") with an equal width of 0.02 ppm over the spectral region between 0.60 and 9.40 ppm by using AMIX 3.9.7 software package (Bruker Biospin, Germany). The region 5.42- 4.38 ppm containing the residual water resonance was excluded, and each integrated region was normalized to the total spectrum area. Hence, a data matrix **X** was created with samples in rows and NMR variables in columns, while class belonging for each sample was encoded into a **Y** matrix. Projection to Latent Structure-Discriminant Analysis (PLS-DA) was then applied to **X** and **Y** matrices, containing control and L-Pro-treated cells data, with SIMCA 14 software (Umetrics, Umeå, Sweden) in order to distinguish cell classes according to the induced metabolite distribution. The obtained statistical model showed R2Y=0.98 and Q2=0.96 (goodness of fit and goodness of prediction, respectively). Acceptable values must be ≥ 0.5 for both, with $|R2 - Q2| < 0.2–0.3$. The robustness of the PLS-DA classification was assessed by permutation test (800 times), which estimated $R2_{fit}$= 0.32 and $Q2_{fit}$=-0.35 suggesting a non-overfitted model. Moreover, CV-ANOVA testing of Cross-Validated predictive residuals was used to assess the reliability of the model obtaining $p=3\times10^{-8}$.

Lactate Activity Assay
Lactate was measured using the colorimetric L-Lactate Assay Kit (Abcam, Cambridge, MA, USA, ab65331), according to the manufacturer's instructions. Data were normalized to total cell number.

Supplemental References

Anders, S., Pyl, P.T., and Huber, W. (2015). HTSeq--a Python framework to work with high-throughput sequencing data. Bioinformatics *31*, 166-169.

Eriksson L, Johansson E, AB. U, Academy U, Kettaneh-Wold N, Wold S. Multi- and Megavariate Data Analysis: Principles and Applications: Umetrics Academy; Umeå, Sweden, 2001.

Fico, A., Manganelli, G., Simeone, M., Guido, S., Minchiotti, G., and Filosa, S. (2008). High-throughput screening-compatible single-step protocol to differentiate embryonic stem cells in neurons. Stem cells and development *17*, 573-584.

Kim, D., Pertea, G., Trapnell, C., Pimentel, H., Kelley, R., and Salzberg, S.L. (2013). TopHat2: accurate alignment of transcriptomes in the presence of insertions, deletions and gene fusions. Genome biology *14*, R36.

Lindon, J.C., Nicholson, J.K., Holmes, E., Keun, H.C., Craig, A., Pearce, J.T., Bruce, S.J., Hardy, N., Sansone, S.A., Antti, H.*, et al.* (2005). Summary recommendations for standardization and reporting of metabolic analyses. Nature biotechnology *23*, 833-838.

Russo, F., and Angelini, C. (2014). RNASeqGUI: a GUI for analysing RNA-Seq data. Bioinformatics *30*, 2514-2516.

Tarazona, S., Garcia-Alcalde, F., Dopazo, J., Ferrer, A., and Conesa, A. (2011). Differential expression in RNA-seq: a matter of depth. Genome research *21*, 2213-2223.

Turro, E., Su, S.Y., Goncalves, A., Coin, L.J., Richardson, S., and Lewin, A. (2011). Haplotype and isoform specific expression estimation using multi-mapping RNA-seq reads. Genome biology *12*, R13.

Wishart, D.S., Tzur, D., Knox, C., Eisner, R., Guo, A.C., Young, N., Cheng, D., Jewell, K., Arndt, D., Sawhney, S.*, et al.* (2007). HMDB: the Human Metabolome Database. Nucleic Acids Res *35*, D521-526.